Research Article

Nano Research
2023, 16(7): 10684–10689

ISSN 1998-0124 CN 11-5974/O4
https://doi.org/10.1007/s12274-023-5697-8

Ultrafast growth of wafer-scale fold-free bilayer graphene

Jilin Tang[1,2,3], Yuechen Wang[1,2,3], Yuwei Ma[4], Xiaoyin Gao[1], Xin Gao[1,2,3], Ning Li[5], Yani Wang[1,3], Shishu Zhang[1], Liming Zheng[1,3], Bing Deng[1,3], Rui Yan[3], Yisen Cao[3], Ronghua Zhang[3], Lianming Tong[1], Jin Zhang[1,2,3], Peng Gao[5], Zhongfan Liu[1,2,3], Xiaoding Wei[4], Hongtao Liu[1] (✉), and Hailin Peng[1,2,3] (✉)

[1] *Center for Nanochemistry, Beijing Science and Engineering Centre for Nanocarbons, Beijing National Laboratory for Molecular Sciences, College of Chemistry and Molecular Engineering, Peking University, Beijing 100871, China*
[2] *Academy for Advanced Interdisciplinary Studies, Peking University, Beijing 100871, China*
[3] *Beijing Graphene Institute, Beijing 100095, China*
[4] *State Key Laboratory for Turbulence and Complex System, Department of Mechanics and Engineering Science, College of Engineering, Beijing Innovation Center for Engineering Science and Advanced Technology, Peking University, Beijing 100871, China*
[5] *Electron Microscopy Laboratory, School of Physics, International Center for Quantum Materials, Peking University, Beijing 100871, China*

Received: 29 December 2022 / **Revised:** 21 March 2023 / **Accepted:** 28 March 2023

ABSTRACT

Bilayer graphene provides a versatile platform for exploring a variety of intriguing phenomena and shows much promise for applications in electronics, optoelectronics, etc. Controlled growth of large-area bilayer graphene is therefore highly desired yet still suffers from a slow growth rate and poor layer uniformity. Meanwhile, graphene wrinkles, including folds and ripples, form during cooling due to the thermal contraction mismatch between graphene and the metal substrates, and have been far from suppressed or eliminated, especially in bilayer graphene, which would greatly degrade the extraordinary properties of graphene. Here we report the ultrafast growth of wafer-scale fold-free bilayer graphene by chemical vapor deposition. Through well-tuning the alloy thickness and strain regulation of the single-crystal CuNi(111)/sapphire, the full coverage of a 2-inch fold-free bilayer graphene wafer via mainly isothermal segregation has been achieved as fast as 30 s. The tensile-strained CuNi(111) film reduces the thermal contraction mismatch and suppresses the formation of graphene folds during cooling, which is directly observed through *in situ* optical microscopy. The ultraflat bilayer graphene exhibits wafer-scale uniformity in electrical performance and enhanced mechanical property comparable to the exfoliated ones. Our results offer a promising route for large-scale production of bilayer graphene and enable its various applications.

KEYWORDS

bilayer graphene, graphene wrinkles, ultrafast growth, *in situ* optical microscopy, single crystal wafer

1 Introduction

Bilayer graphene (BLG), with various interlayer-angle-dependent novel electrical properties [1], as well as superior mechanical strength [2] and electrical conductivity [3] compared to monolayer graphene (MLG), has attracted wide interest. It can be produced mainly by mechanical exfoliation [4], artificially stacking two layers of monolayer graphene [5], and chemical vapor deposition (CVD) [6]. Among those, the CVD approach shows a capability of producing high-quality BLG and promising scalability. Large-area BLG has been synthesized by CVD on a variety of metallic substrates, such as Cu [7, 8], CuNi [9–12], CuSi [13], and other alloy substrates [14]. However, BLG grown on metal substrates such as Cu and CuNi foils usually suffers from poor layer number uniformity, strong surface corrugation, and wrinkles, which may cause anisotropic electrical properties [15, 16], reduced mechanical strength/thermal conductivity [17, 18], and degraded anticorrosion performance [19]. On the other hand, the growth mechanism of BLG on carbon-solvable substrates such as CuNi has not been directly investigated in real-time, and it usually takes tens to hundreds of minutes to obtain fully covered wafer-scale BLG [9, 12].

Graphene wrinkles, including ripples and folds, form during the growth and/or transfer process. Ripples are induced mainly by the metal substrate surface corrugation and can be released by the reformative transfer method [20]. Whereas the intrinsic folds, forming during the growth, are graphene layers buckling together or even falling over. They mainly originate from the interfacial compressive strain relaxation caused by the difference in the coefficient of thermal expansion (CTE) between graphene and the metal substrate during cooling. The relaxation of interfacial compressive strain leads to substrate step bunching in one direction and graphene detachment and fold formation in the perpendicular direction [21, 22]. Besides, step bunching is also believed to be driven by the release of graphene bending energy [23], further triggering the graphene detachment and fold formation [22]. Unlike graphene ripples, folds in graphene are impossible to release by transfer. Therefore, it is important to eliminate the fold at the growth stage and grow fold-free graphene.

Several approaches have been proposed to eliminate the wrinkles in graphene, particularly in monolayer graphene, such as using substrates with a small difference in CTE [24, 25], or lowering the growth temperature to avoid the abrupt step

Address correspondence to Hongtao Liu, htliu-cnc@pku.edu.cn; Hailin Peng, hlpeng@pku.edu.cn

bunching and fold formation [22, 26]. Our group has reported that using Cu(111) thin film which has a relatively small difference in CTE and relatively strong coupling to graphene, can eliminate wrinkles in monolayer graphene [16]. The flat nature of the epitaxial Cu(111) film also prevents the directional diffusion of Cu atoms underlying graphene and suppresses the step bunching [18]. In contrast, step bunching and wrinkles in BLG develop more pronouncedly than those in monolayer graphene (Fig. S1 in the Electronic Supplementary Material (ESM)) [27], which, to the best of our knowledge, has been far less addressed.

Herein, we report the ultrafast growth of fold-free BLG on a strain-regulated single-crystal CuNi(111) thin film epitaxially deposited on α-Al_2O_3(0001) (sapphire) wafer. The CuNi(111) film thickness is well optimized to achieve rapid growth of 2-inch fully-covered BLG wafers within 30 s. Optical microscopy (OM), scanning electron microscopy (SEM), and atomic force microscopy (AFM) confirm the fold-free nature of the obtained BLG wafer. *In situ* optical microscopy studies directly reveal the isothermal segregation growth of graphene as well as the suppression of fold formation in BLG during cooling. The suppression of fold formation is attributed to the limited substrate surface reconstruction (i.e., step bunching), in which the tensile strain imposed on the CuNi(111) film by sapphire during cooling and the flat nature of the CuNi(111) surface play an important role. The fold-free BLG film exhibits wafer-scale uniformity in electrical performance and enhanced mechanical property comparable to the exfoliated ones.

2 Results and discussion

Wafer-scale uniform fold-free BLG was grown on single-crystal CuNi(111) film substrates epitaxial on sapphire(0001) wafers as illustrated in Fig. 1(a). The single-crystal CuNi(111) films were prepared by sputtering Ni on twin-free single-crystal Cu(111) thin films. Subsequent annealing results in twin-free single-crystal CuNi(111) films with Cu/Ni atomic ratio of 80/20 (Fig. S2 in the ESM). BLG grows on the CuNi alloy substrate via mainly the isothermal segregation instead of the carbon precipitation, the latter of which arises from the decrease in carbon solubility upon cooling. During isothermal segregation growth of graphene, the CuNi substrate acts as a carbon reservoir, in which the carbon concentration remains dynamically constant at a certain growth temperature. Carbon dissolves at bare CuNi and segregates under the monolayer graphene covered region, forming the second layer of graphene (Figs. S3 and S4 in the ESM) [28]. *In situ* study of the BLG growth under an optical microscope indicates that the growth of the bottom second layer graphene stops as long as the top graphene layer covers the entire catalytic CuNi surface (Figs. S5 and S6 in the ESM, and Video ESM1). Layer sequence of the BLG was confirmed to be the "inverted wedding cake" structure by *in situ* etching experiment (Figs. S7 and S8 in the ESM and Video ESM2) [11]. In order to grow fully-covered BLG, the carbon supply rate through isothermal segregation must be fast enough before the catalytic surface is fully covered. The substrate thickness at a given Ni concentration is found to be crucial for controlling the carbon supply rate and growing uniform of BLG. The optimized thickness of CuNi(111) film is 500 nm for the growth of uniform BLG (Fig. S9 in the ESM). 2-inch BLG film can be grown on the CuNi(111)/sapphire in a 3-inch CVD tube furnace within 30 s (Fig. 1(b)), which was confirmed by capturing the growth process at different growth stages (Figs. 1(c)–1(e) and Fig. S10 in the ESM) and the isotope labeling experiments (Fig. S11 in the ESM). Benefiting from the fast carbon supply brought by the ultra-thin substrate, the growth rate of BLG domains on $Cu_{80}Ni_{20}$(111) thin films reaches 140 μm·min^{-1} (Figs. 1(c)–1(e)), 14 times faster than the growth rate of BLG on CuNi foil (~ 10 μm·min^{-1}) [11] and 28 times faster than that of BLG on Cu foil (~ 5 μm·min^{-1}) [29].

Generally, graphene folds generate during cooling from the growth temperature to room temperature (RT) due to the

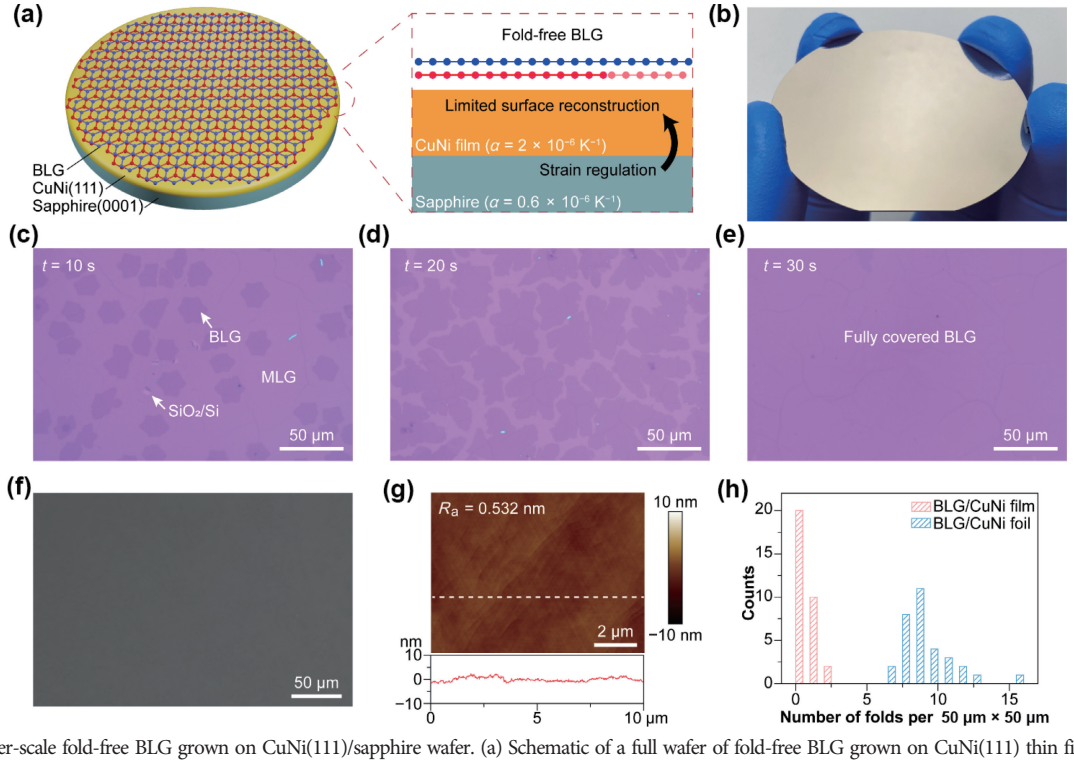

Figure 1 Wafer-scale fold-free BLG grown on CuNi(111)/sapphire wafer. (a) Schematic of a full wafer of fold-free BLG grown on CuNi(111) thin film epitaxial on sapphire. The inset is the cross-section of the wafer. BLG including AB-BLG and tBLG grows on strain-regulated CuNi(111)/sapphire. (b) Photograph of a 2-inch BLG/CuNi(111)/sapphire wafer. (c)–(e) OM images of graphene captured during different growth stages, 10 s (c), 20 s (d) and 30 s (e). (f) SEM image of the BLG grown on CuNi(111)/sapphire. (g) Typical AFM image of fold-free BLG on CuNi(111)/sapphire substrate. The bottom inset shows the height profile along the white dashed line in the AFM image. (h) Histogram of the fold numbers per 50 μm × 50 μm from optical images of BLG grown on CuNi(111)/sapphire and CuNi(111) foil.

mismatch of the CTE between graphene and the metal substrate [22]. While in our BLG/CuNi wafer, since the CTE of the sapphire ($\alpha_{sapphire}$ = 7.3 × 10^{-6} K^{-1}) [30], the substrate of the CuNi film, is smaller than that of CuNi film (α_{CuNi} = 16.6 × 10^{-6} K^{-1}) [31], a tensile stress is imposed on the CuNi film during cooling, preventing it from strong surface reconstruction (i.e., step bunching) and hindering the fold formation in graphene. The details of the CuNi surface reconstruction and graphene fold formation will be discussed later. A significantly lower density of fold in our BLG/CuNi wafer was confirmed by SEM (Fig. 1(f)), AFM (Fig. 1(g)) and fold statistical analysis compared to BLG/CuNi foil (Fig. 1(h)). As shown in Fig. 1(f), the SEM image shows uniform contrast over 200 μm × 300 μm, indicating no fold in the as-grown BLG. The root-mean-square roughness (R_a) of the BLG/CuNi(111)/sapphire is as small as 0.532 nm (Fig. 1(g)). Further investigation of 25 AFM images over a 2-inch wafer shows the wafer-scale flatness of our BLG wafer (Fig. S12 in the ESM). There is almost no fold in BLG grown on CuNi(111)/sapphire (Fig. 1(h)), while there are ~ 8 folds per 50 μm × 50 μm in BLG grown on CuNi(111) foil. Through the substrate modulation mentioned above, including thickness and strain regulation of the CuNi(111) film, rapid synthesis of wafer-scale fold-free BLG can be achieved.

To characterize the uniformity and crystallinity of the BLG wafer, the as-grown 2-inch BLG was transferred onto a 4-inch SiO_2/Si wafer (Fig. 2(a)). Raman mapping was performed on a randomly chosen 100 μm × 100 μm region. The G band intensity map shows a uniform contrast indicating high uniformity of layer number of the BLG film (Fig. 2(b)). Raman map of I_D/I_G (Fig. 2(c)) together with the 15 representative Raman spectra (Fig. 2(d)) across the 2-inch graphene shows no existence of D band, indicating the high crystallinity of the BLG film. The emergence of R' band and G band variation stem from twisted bilayer graphene (tBLG) with non-AB stacking structure (mainly 5° and 30° tBLG). Two representative high-angle annular dark-field scanning transmission electron microscopy (HAADF-STEM) images of our bilayer graphene indicate a clear lattice structure (Figs. 2(e) and 2(f)). The two STEM images also show different stacking structures, including AB-BLG (Fig. 2(e)) and tBLG (Fig. 2(f)) with an interlayer twist angle of 5.8°. The ratio of the AB-BLG is statistically calculated to be 66% and that of tBLG is 34% based on 100 selected area electron diffraction (SAED) patterns within a 3 mm TEM grid (Fig. 2(g)). Both Raman and STEM data indicate that the BLG has high quality and contains different stacking orders besides the AB stacking.

To address the origin of the suppression of graphene fold formation on our strain-regulated CuNi(111)/sapphire substrate, the morphology evolution of BLG/metal substrates upon cooling was studied in real-time under an optical microscope in an *in situ* CVD system (Fig. S5 in the ESM). Real time videos were recorded to capture the cooling process of BLG grown on both the CuNi(111)/sapphire (Video ESM3) and CuNi(111) foil (Video ESM4), which were subjected to cooling from 1253 K to RT at 30 K·min^{-1}. When the BLG/metal substrates are cooled from 1253 K to RT, the sapphire shrinks less upon cooling than the CuNi film on it, which simultaneously exerts tensile stress on the CuNi film. To release the large tensile stress, the CuNi film has to yield through plastic deformation. As for the face-centered cubic (FCC) CuNi(111) film, the plastic deformation mainly occurs by slipping along the close-packed {111} glide planes, forming dense monoatomic steps on the crystal surface. Actually, such slip-induced atomic steps can be widely observed in our CuNi(111) film (Fig. S13 in the ESM), consistent with other reports [16, 18, 32], indicating the occurrence of the tensile deformation in the CuNi film during cooling. Thus, CuNi film can follow the thermal contraction of the sapphire and shrink less than the freely shrinking CuNi foil, which substantially suppresses the fold formation of graphene on CuNi(111)/sapphire. The tensile strain counteracts the cooling-induced compressive strain, together with the atomically flat CuNi(111) surface, impeding the interfacial compressive strain relaxation and preventing the CuNi film from step bunching, which usually triggers the graphene detachment and fold formation [18, 22] (Fig. 3(a)). In contrast, step bunches and perpendicular graphene folds form on the freely contracted BLG/CuNi foil upon cooling as a consequence of unobstructed compressive strain relaxation (Fig. 3(b)).

The OM image of the BLG/CuNi(111)/sapphire taken at RT after the cooling process (Fig. 3(c)) shows a uniformly flat surface without any apparent step bunching and graphene fold. The flat surface is also confirmed by the optical intensity profile along the blue dashed line in the OM image, which exhibits no step bunches. However, step bunches and graphene fold can be clearly seen in BLG/CuNi(111) foil at RT, as shown in Fig. 3(d). The optical intensity profile shows strong fluctuation at the BLG-

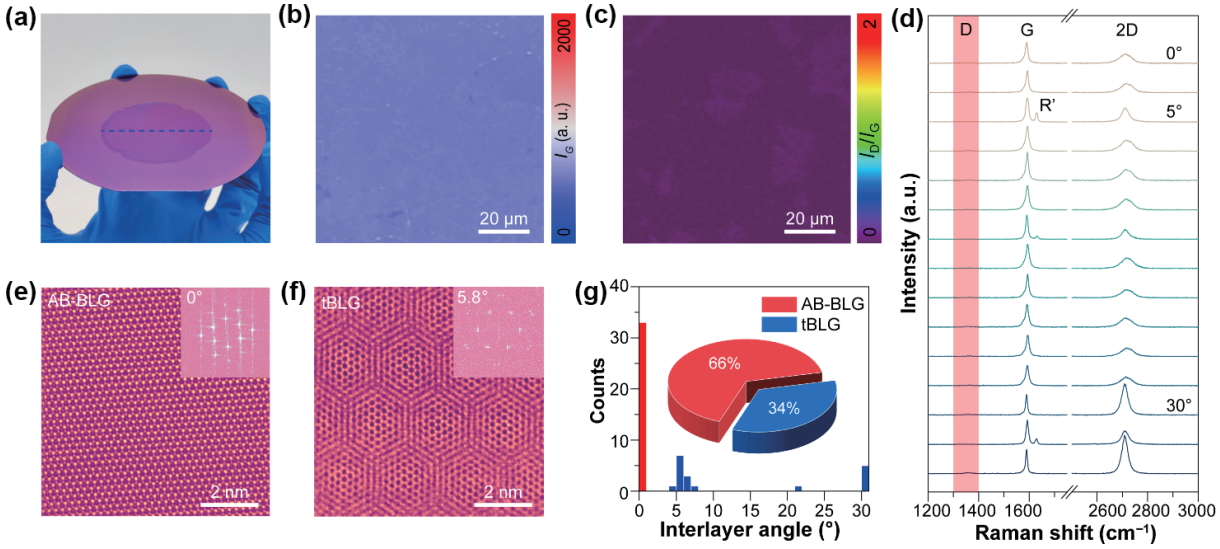

Figure 2 Structural characterizations of BLG. (a) Photograph of a 2-inch BLG transferred onto a 4-inch SiO_2/Si wafer. (b) and (c) Raman map of the G band (b) and I_D/I_G (c) in a randomly selected region of 100 μm × 100 μm. (d) Raman spectra of 15 spots across the 2-inch BLG along the blue dash line in (a). (e) and (f) Atomic-resolution STEM images of BLG with AB stacking (e) and a twisted interlayer angle (f). (g) Statistical histogram of the twist angle distribution of the as-grown BLG. The inset is the pie chart showing the ratio of AB-BLG and tBLG.

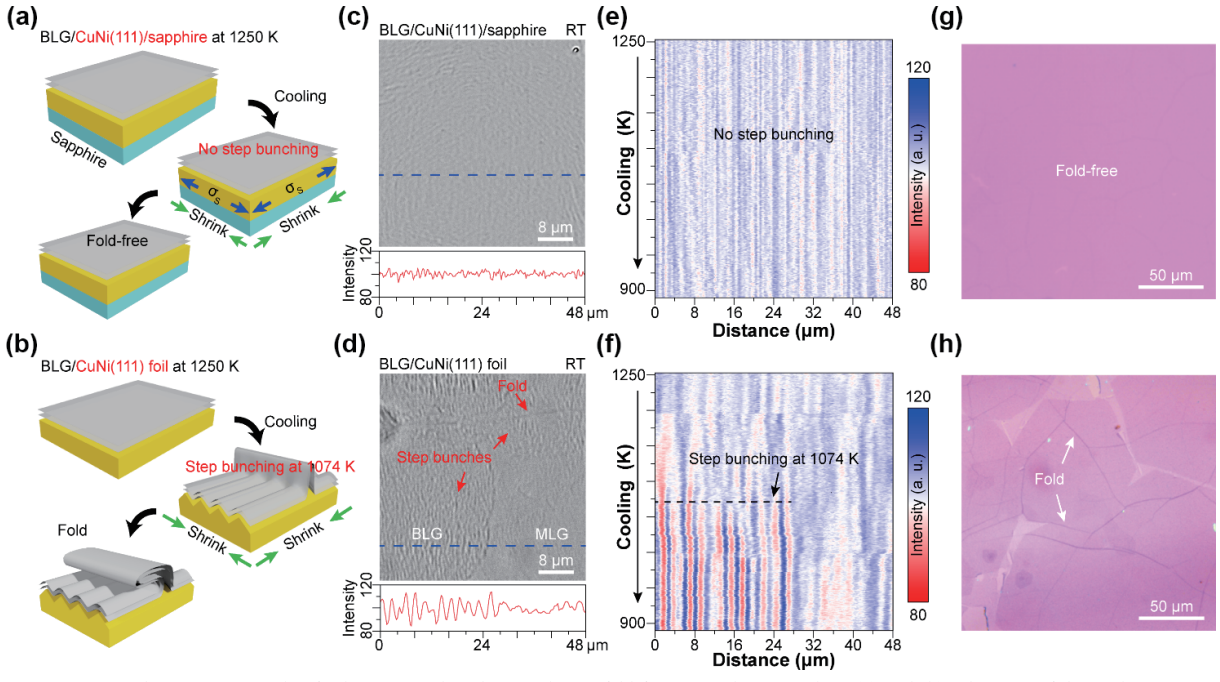

Figure 3 *In situ* optical microscopy study of substrate step bunching and BLG fold formation during cooling. (a) and (b) Schematic of the cooling process of the BLG/CuNi(111)/sapphire (a) and (b) BLG/CuNi(111) foil. (c) and (d) Snapshot of the BLG/CuNi(111)/sapphire (c) and BLG/CuNi(111) foil (d) taken at RT. The bottom insets show the optical intensity profile along the blue dashed lines in the OM images. (e) and (f) Corresponding optical intensity evolution during cooling from 1253 to 890 K. (g) and (h) OM images of BLG grown on CuNi(111)/sapphire (g) and CuNi(111) foil (h) transferred onto SiO_2/Si.

covered region, reflecting the wide and tall step bunch structure. The optical intensity profile of BLG/CuNi(111)/sapphire and BLG/CuNi(111) foil are further plotted against temperature to investigate the surface morphology changes during the cooling process, respectively (Figs. 3(e) and 3(f)). The optical intensity of BLG/CuNi(111)/sapphire does not change with decreasing temperature from 1253 to 890 K, indicating no step bunching occurs. In contrast, step bunching can be clearly observed around 1074 K in the BLG/CuNi foil, which is consistent with previous reports [22, 23]. The fold-free feature of the BLG grown on CuNi(111)/sapphire can also be identified after being transferred onto SiO_2/Si substrate, as shown in Fig. 3(g), which is quite different from that grown on CuNi(111) foil with several folds in it (Fig. 3(h)).

Owing to the high layer uniformity and fold-free flat surface, BLG shows uniform electrical performance. The sheet resistance of a 2-inch wafer-sized BLG is 344 ± 39 (11%) Ω·sq^{-1} (Fig. 4(a)) with a narrow sheet resistance distribution (Fig. 4(b)). The mechanical properties of graphene are highly sensitive to wrinkles [18]. Therefore, we investigated the mechanical properties of fold-free BLG utilizing the AFM nanoindentation technique [33]. The samples to be tested were first transferred onto a SiO_2/Si substrate with pre-patterned circular holes for the indentation test. Wrinkled MLG and BLG grown on Cu foil were tested for comparison as well. The typical load-indentation depth curves of graphene are shown in Fig. 4(c), from which the two-dimensional (2D) Young's modulus (E^{2D}) and 2D breaking strength (σ^{2D}) of graphene can be extracted [34]. The 2D Young's modulus and 2D breaking strength of fold-free BLG are estimated to be 693 and 78 N·m^{-1}, corresponding to a bulk Young's modulus of 1.03 TPa and breaking strength of 116 GPa, close to the values of the exfoliated one [14, 34]. While the wrinkled MLG (E^{2D} ~ 187 N·m^{-1} and σ^{2D} ~ 28 N·m^{-1}) and BLG (E^{2D} ~ 408 N·m^{-1} and σ^{2D} ~ 44 N·m^{-1}) show a much weaker mechanical strength.

The enhanced mechanical strength of fold-free BLG can also be corroborated in practical application scenarios. A wet transfer method was intentionally adopted to transfer the graphene onto a holey SiO_2/Si substrate, which involved hot liquid acetone immersion to mimic the harsh device manufacturing process (see details in the Experimental section). Almost 98% of the suspended fold-free BLG survived the large surface tension during the acetone immersion and drying process. By contrast, the mean intactness of suspended MLG is only ~ 53%, and that of suspended BLG with folds is ~ 69% (Fig. 4(d)). Such a strong yet atomically thin membrane with uniform and high electrical conductivity could pave the way toward practical applications of graphene.

3 Conclusions

To conclude, ultrafast growth of wafer-scale fold-free BLG with layer homogeneity has been achieved on a strain-regulated single-crystal CuNi(111)/sapphire substrate. As-grown BLG possesses high crystal quality, confirmed by Raman and STEM. *In situ* optical microscopy reveals the ultrafast isothermal segregation growth of BLG as well as the suppression of the substrate step bunching and BLG fold formation on the tensile-strained CuNi(111)/sapphire substrate during cooling. As-grown BLG exhibits uniform electrical conductivity with a sheet resistance of 344 ± 39 (11%) Ω·sq^{-1} and high mechanical strength (E^{2D} ~ 693 N·m^{-1} and σ^{2D} ~ 78 N·m^{-1}) comparable to that of exfoliated graphene and better than the wrinkled ones. The enhanced mechanical strength of fold-free BLG gives rise to the high intactness of the suspended BLG array transferred onto a holey SiO_2/Si substrate. This work not only provides a fundamental understanding of BLG growth on CuNi substrate and fold formation in BLG, but also paves the way to the wafer-scale integration and applications of BLG films.

4 Method

Preparation of single-crystal CuNi(111) film: Typically, Cu film (thickness ~ 400 nm) was deposited on an oxygen-annealed single-crystal sapphire (2 in., *c* plane with miscut < 0.5°, 650 μm thickness, Epi-ready with R_a < 0.2 nm) by a direct current (DC) sputtering technique using a physical vapor deposition (PVD)

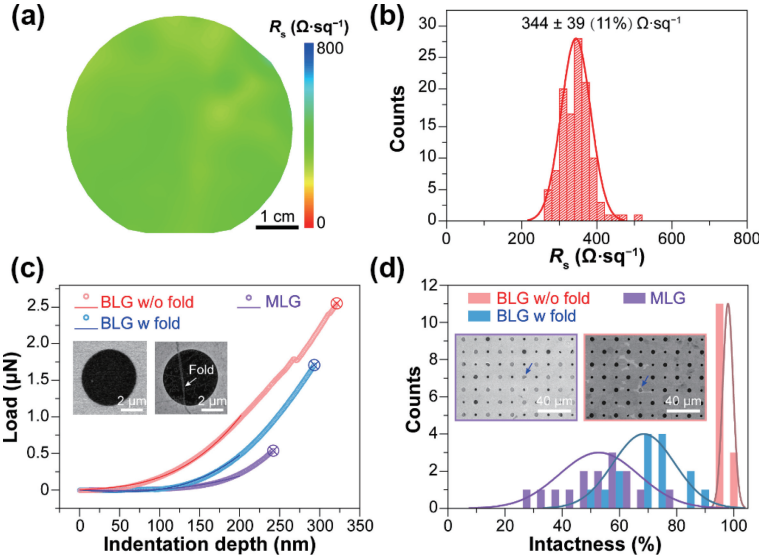

Figure 4 Electrical and mechanical properties of BLG grown on CuNi(111)/sapphire wafer. (a) and (b) Sheet resistance map of a 2-inch BLG wafer (a) and its corresponding statistical distribution (b). (c) Typical load-displacement curves of the suspended MLG and BLG with and without fold obtained from AFM nanoindentation tests. Solid lines are the fitting curves. The insets are SEM images of the suspended BLG with (right panel) and without fold (left panel), in which the fold is indicated by the white arrow. (d) Statistical histogram of the intactness of suspended MLG and BLG with and without fold transferred onto holey SiO_2/Si substrates. The insets are SEM images of suspended MLG (left panel) and BLG without fold (right panel), in which the bright contrast (blue arrows) indicates broken holes.

equipment (ULVAC, QAM-4W). A DC power of 200 W was applied to deposit Cu film at 0.3 nm·s^{-1}, with a base pressure of 5.6×10^{-5} Pa. The Cu/sapphire was further annealed at 1273 K with 500 standard cubic centimeters per minute (sccm) Ar and 10 sccm H_2 at atmospheric pressure for 1 h to obtain highly crystalline twin-free Cu(111)/sapphire. Then 100 nm-thick Ni thin film was deposited on the single-crystal Cu(111)/sapphire. The Ni/Cu(111)/sapphire was alloyed at 1273 K with 500 sccm Ar and 10 sccm H_2 at atmospheric pressure for 1 h, resulting in a twin-free single-crystal CuNi(111) wafer with Ni concentration of 20%. CuNi(111) films with different thicknesses at 20% Ni concentration can be obtained by adjusting the thicknesses of the Cu and Ni layers accordingly.

Graphene growth and transfer: The 2-inch CuNi(111)/sapphire was heated to 1273 K with 460 sccm Ar at 4500 Pa in a 3-inch quartz tube furnace. Then 2.5 sccm CH_4 and 110 sccm H_2 were introduced for graphene growth. After 30 s growth of graphene, CH_4 gas flow was switched off and the sample was pulled out from the heating zone immediately and cooled to RT. To transfer graphene, a thin film of polymethyl methacrylate (PMMA) (4 wt.% in anisole, 950 K, 2000 rpm for 1 min) was spin-coated onto the graphene/CuNi substrate. After baking at 170 °C for 3 min, the PMMA/graphene/CuNi was put into a 1 M ammonium persulfate ($(NH_4)_2S_2O_8$) aqueous solution. After etching, the PMMA/graphene was rinsed in DI water several times and attached to the SiO_2/Si substrate. Following overnight drying, the PMMA layer was dissolved by hot acetone, leaving the graphene film on the SiO_2/Si substrate. For the nanoindentation test and fabrication of the suspended graphene array, the PMMA/graphene was scooped by a polyethylene terephthalate (PET) frame and dried. Then it was placed onto SiO_2/Si substrates with prepatterned array wells. The PMMA layer was further removed by immersing the sample in hot acetone.

Characterization: Optical microscopy was conducted on a Nikon LV150. Raman spectra of transferred graphene were collected on a Witec alpha RAS300+ Raman system using a 488 nm laser with a laser spot size of 1 μm, and a 100× objective and 600 lines/mm grating were used to collect the Raman signal. SEM images were obtained on a Hitachi S4800 field-emission scanning electron microscope. Electron backscattering diffraction (EBSD) and energy dispersive spectroscopy (EDS) measurements were carried out on a Thermo Scientific Quattro S system equipped with the EBSD probe (AMETEK EDAX DigitalView EBSD Camera in combination with EDAX's TEAM) and EDS probe (AMETEK EDAX Octane Elect EDS System). TEM characterizations were conducted using a FEI Tecnai F20 for collecting SAED patterns under 200 kV. The aberration-corrected STEM images of graphene were performed using a Nion U-HERMS200 microscope at 60 kV. White light interferometry (WLI) images were conducted using a Nikon white light interferometer (BW-M7000). The AFM morphology images were collected on a Brucker Dimension Icon using the ScanAsyst mode. The nano-indentation experiment was performed using Asylum Cypher ES AFM. The sheet resistances of transferred 2-inch graphene wafers were collected by a CDE ResMap 178 four-probe resistance tester.

In situ optical microscopy: The *in situ* optical microscopy study was conducted based on a high-temperature reactor (Linkam Scientific Instruments, CCR1000) equipped with a custom-made vacuum and gas (Ar, H_2, CH_4) supply system. A transparent quartz window installed on top of the reactor provided optical access for *in situ* study. The reactor was mounted under a reflective optical microscope (Nikon Eclipse LV150) equipped with a DS-Ri 2 camera. A 50× lens with a working distance of 10 mm was used to collect the reflected light. The above system is capable of providing temperatures up to 1253 K and gas pressure from 10 to 500,000 Pa. The temperature at the sample position was calibrated by the melting point of Ag (Fig. S14 in the ESM). The captured images/videos were converted to grayscale, and the contrast was enhanced.

Acknowledgements

This work was supported by the National Natural Science Foundation of China (Nos. 52021006, T2188101, and 22105009), Beijing National Laboratory for Molecular Sciences (No. BNLMS-CXTD-202001), and the Tencent Foundation (No. XPLORER PRIZE). We acknowledge Molecular Materials and Nanofabrication Laboratory (MMNL) in the College of Chemistry at Peking University for the use of instruments.

Electronic Supplementary Material: Supplementary material (further details of the graphene fold structure analysis, characterizations of the CuNi(111)/sapphire substrates, isothermal growth mechanism of graphene, *in situ* optical microscopy apparatus, isotope labeling experiments, *in situ* etching experiment, flatness of a 2-inch BLG/CuNi(111)/sapphire wafer, thermal contraction analysis of the CuNi(111)/sapphire and the temperature calibration of the *in situ* apparatus as well as the *in situ* videos of BLG growth and cooling processes) is available in the online version of this article at https://doi.org/10.1007/s12274-023-5697-8.

References

[1] Cao, Y.; Fatemi, V.; Fang, S. A.; Watanabe, K.; Taniguchi, T.; Kaxiras, E.; Jarillo-Herrero, P. Unconventional superconductivity in magic-angle graphene superlattices. *Nature* **2018**, *556*, 43–50.

[2] Lin, Q. Y.; Zeng, Y. H.; Liu, D.; Jing, G. Y.; Liao, Z. M.; Yu, D. P. Step-by-step fracture of two-layer stacked graphene membranes. *ACS Nano* **2014**, *8*, 10246–10251.

[3] Bae, S.; Kim, H.; Lee, Y.; Xu, X. F.; Park, J. S.; Zheng, Y.; Balakrishnan, J.; Lei, T.; Kim, H. R.; Song, Y. I. et al. Roll-to-roll production of 30-inch graphene films for transparent electrodes. *Nat. Nanotechnol.* **2010**, *5*, 574–578.

[4] Novoselov, K. S.; Jiang, D.; Schedin, F.; Booth, T. J.; Khotkevich, V. V.; Morozov, S. V.; Geim, A. K. Two-dimensional atomic crystals. *Proc. Natl. Acad. Sci. USA* **2005**, *102*, 10451–10453.

[5] Nguyen, V. L.; Perello, D. J.; Lee, S.; Nai, C. T.; Shin, B. G.; Kim, J. G.; Park, H. Y.; Jeong, H. Y.; Zhao, J.; Vu, Q. A. et al. Wafer-scale single-crystalline AB-stacked bilayer graphene. *Adv. Mater.* **2016**, *28*, 8177–8183.

[6] Liu, L. X.; Zhou, H. L.; Cheng, R.; Yu, W. J.; Liu, Y.; Chen, Y.; Shaw, J.; Zhong, X.; Huang, Y.; Duan, X. F. High-yield chemical vapor deposition growth of high-quality large-area AB-stacked bilayer graphene. *ACS Nano* **2012**, *6*, 8241–8249.

[7] Wang, H. Z.; Yao, Z. P.; Jung, G. S.; Song, Q. C.; Hempel, M.; Palacios, T.; Chen, G.; Buehler, M. J.; Aspuru-Guzik, A.; Kong, J. Frank-van der Merwe growth in bilayer graphene. *Matter* **2021**, *4*, 3339–3353.

[8] Hao, Y. F.; Wang, L.; Liu, Y. Y.; Chen, H.; Wang, X. H.; Tan, C.; Nie, S.; Suk, J. W.; Jiang, T. F.; Liang, T. F. et al. Oxygen-activated growth and bandgap tunability of large single-crystal bilayer graphene. *Nat. Nanotechnol.* **2016**, *11*, 426–431.

[9] Takesaki, Y.; Kawahara, K.; Hibino, H.; Okada, S.; Tsuji, M.; Ago, H. Highly uniform bilayer graphene on epitaxial Cu-Ni(111) alloy. *Chem. Mater.* **2016**, *28*, 4583–4592.

[10] Gao, Z. L.; Zhang, Q. C.; Naylor, C. H.; Kim, Y.; Abidi, I. H.; Ping, J. L.; Ducos, P.; Zauberman, J.; Zhao, M. Q.; Rappe, A. M. et al. Crystalline bilayer graphene with preferential stacking from Ni-Cu gradient alloy. *ACS Nano* **2018**, *12*, 2275–2282.

[11] Huang, M.; Bakharev, P. V.; Wang, Z. J.; Biswal, M.; Yang, Z.; Jin, S.; Wang, B.; Park, H. J.; Li, Y. Q.; Qu, D. S. et al. Large-area single-crystal AB-bilayer and ABA-trilayer graphene grown on a Cu/Ni(111) foil. *Nat. Nanotechnol.* **2020**, *15*, 289–295.

[12] Solis-Fernandez, P.; Terao, Y.; Kawahara, K.; Nishiyama, W.; Uwanno, T.; Lin, Y. C.; Yamamoto, K.; Nakashima, H.; Nagashio, K.; Hibino, H. et al. Isothermal growth and stacking evolution in highly uniform bernal-stacked bilayer graphene. *ACS Nano* **2020**, *14*, 6834–6844.

[13] Nguyen, V. L.; Duong, D. L.; Lee, S. H.; Avila, J.; Han, G.; Kim, Y. M.; Asensio, M. C.; Jeong, S. Y.; Lee, Y. H. Layer-controlled single-crystalline graphene film with stacking order via Cu-Si alloy formation. *Nat. Nanotechnol.* **2020**, *15*, 861–867.

[14] Ma, W.; Chen, M. L.; Yin, L. C.; Liu, Z. B.; Li, H.; Xu, C.; Xin, X.; Sun, D. M.; Cheng, H. M.; Ren, W. C. Interlayer epitaxy of wafer-scale high-quality uniform AB-stacked bilayer graphene films on liquid Pt_3Si/solid Pt. *Nat. Commun.* **2019**, *10*, 2809.

[15] Zhu, W. J.; Low, T.; Perebeinos, V.; Bol, A. A.; Zhu, Y.; Yan, H. G.; Tersoff, J.; Avouris, P. Structure and electronic transport in graphene wrinkles. *Nano Lett.* **2012**, *12*, 3431–3436.

[16] Deng, B.; Pang, Z. Q.; Chen, S. L.; Li, X.; Meng, C. X.; Li, J. Y.; Liu, M. X.; Wu, J. X.; Qi, Y.; Dang, W. H. et al. Wrinkle-free single-crystal graphene wafer grown on strain-engineered substrates. *ACS Nano* **2017**, *11*, 12337–12345.

[17] Chen, S. S.; Li, Q. Y.; Zhang, Q. M.; Qu, Y.; Ji, H. X.; Ruoff, R. S.; Cai, W. W. Thermal conductivity measurements of suspended graphene with and without wrinkles by micro-Raman mapping. *Nanotechnology* **2012**, *23*, 365701.

[18] Deng, B.; Hou, Y.; Liu, Y.; Khodkov, T.; Goossens, S.; Tang, J. L.; Wang, Y. N.; Yan, R.; Du, Y.; Koppens, F. H. L. et al. Growth of ultraflat graphene with greatly enhanced mechanical properties. *Nano Lett.* **2020**, *20*, 6798–6806.

[19] Zhang, Y. H.; Wang, B.; Zhang, H. R.; Chen, Z. Y.; Zhang, Y. Q.; Wang, B.; Sui, Y. P.; Li, X. L.; Xie, X. M.; Yu, G. H. et al. The distribution of wrinkles and their effects on the oxidation resistance of chemical vapor deposition graphene. *Carbon* **2014**, *70*, 81–86.

[20] Wang, B.; Huang, M.; Tao, L.; Lee, S. H.; Jang, A. R.; Li, B. W.; Shin, H. S.; Akinwande, D.; Ruoff, R. S. Support-free transfer of ultrasmooth graphene films facilitated by self-assembled monolayers for electronic devices and patterns. *ACS Nano* **2016**, *10*, 1404–1410.

[21] Deng, B.; Wu, J. X.; Zhang, S. S.; Qi, Y.; Zheng, L. M.; Yang, H.; Tang, J. L.; Tong, L. M.; Zhang, J.; Liu, Z. F. et al. Anisotropic strain relaxation of graphene by corrugation on copper crystal surfaces. *Small* **2018**, *14*, 1800725.

[22] Wang, M. H.; Huang, M.; Luo, D.; Li, Y. Q.; Choe, M.; Seong, W. K.; Kim, M.; Jin, S.; Wang, M. R.; Chatterjee, S. et al. Single-crystal, large-area, fold-free monolayer graphene. *Nature* **2021**, *596*, 519–524.

[23] Yi, D.; Luo, D.; Wang, Z. J.; Dong, J. C.; Zhang, X.; Willinger, M. G.; Ruoff, R. S.; Ding, F. What drives metal-surface step bunching in graphene chemical vapor deposition. *Phys. Rev. Lett.* **2018**, *120*, 246101.

[24] Lee, J. H.; Lee, E. K.; Joo, W. J.; Jang, Y.; Kim, B. S.; Lim, J. Y.; Choi, S. H.; Ahn, S. J.; Ahn, J. R.; Park, M. H. et al. Wafer-scale growth of single-crystal monolayer graphene on reusable hydrogen-terminated germanium. *Science* **2014**, *344*, 286–289.

[25] Choi, J. K.; Kwak, J.; Park, S. D.; Yun, H. D.; Kim, S. Y.; Jung, M.; Kim, S. Y.; Park, K.; Kang, S.; Kim, S. D. et al. Growth of wrinkle-free graphene on texture-controlled platinum films and thermal-assisted transfer of large-scale patterned graphene. *ACS Nano* **2015**, *9*, 679–686.

[26] Zhang, X. F.; Wu, T. R.; Jiang, Q.; Wang, H. S.; Zhu, H. L.; Chen, Z. Y.; Jiang, R.; Niu, T. C.; Li, Z. J.; Zhang, Y. W. et al. Epitaxial growth of 6 in. Single-crystalline graphene on a Cu/Ni (111) film at 750 °C via chemical vapor deposition. *Small* **2019**, *15*, 1805395.

[27] Kang, J. H.; Moon, J.; Kim, D. J.; Kim, Y.; Jo, I.; Jeon, C.; Lee, J.; Hong, B. H. Strain relaxation of graphene layers by Cu surface roughening. *Nano Lett.* **2016**, *16*, 5993–5998.

[28] Shelton, J. C.; Patil, H. R.; Blakely, J. M. Equilibrium segregation of carbon to a nickel (111) surface: Surface phase transition. *Surf. Sci.* **1974**, *43*, 493–520.

[29] Gong, P.; Tang, C.; Wang, B. R.; Xiao, T. S.; Zhu, H.; Li, Q. W.; Sun, Z. Z. Precise CO_2 reduction for bilayer graphene. *ACS Cent. Sci.* **2022**, *8*, 394–401.

[30] Yim, W. M.; Paff, R. J. Thermal expansion of AlN, sapphire, and silicon. *J. Appl. Phys.* **1974**, *45*, 1456–1457.

[31] Suh, I. K.; Ohta, H.; Waseda, Y. High-temperature thermal expansion of six metallic elements measured by dilatation method and X-ray diffraction. *J. Mater. Sci.* **1988**, *23*, 757–760.

[32] Zeller, P.; Weinl, M.; Speck, F.; Ostler, M.; Henss, A. K.; Seyller, T.; Schreck, M.; Wintterlin, J. Single crystalline metal films as substrates for graphene growth. *Ann. Der Phys.* **2017**, *529*, 1700023.

[33] Lee, C.; Wei, X. D.; Kysar, J. W.; Hone, J. Measurement of the elastic properties and intrinsic strength of monolayer graphene. *Science* **2008**, *321*, 385–388.

[34] Lee, C.; Wei, X. D.; Li, Q. Y.; Carpick, R.; Kysar, J. W.; Hone, J. Elastic and frictional properties of graphene. *Phys. Status Solidi B* **2009**, *246*, 2562–2567.